New Journal of Physics
The open-access journal for physics

Temperature changes when adiabatically ramping up an optical lattice

Lode Pollet[1,6], **Corinna Kollath**[2,3], **Kris Van Houcke**[4,5] **and Matthias Troyer**[1]

[1] Theoretische Physik, ETH Zürich, 8093 Zürich, Switzerland
[2] Université de Genève, 24 Quai Ernest-Ansermet, CH-1211 Genève, Switzerland
[3] Centre de Physique Théorique, Ecole Polytechnique, CNRS, 91128 Palaiseau Cedex, France
[4] Vakgroep Subatomaire en Stralingsfysica, Proeftuinstraat 86, Universiteit Gent, Belgium
[5] Department of Physics, University of Massachusetts, Amherst, MA 01003, USA
E-mail: pollet@itp.phys.ethz.ch

New Journal of Physics **10** (2008) 065001 (31pp)
Received 15 January 2008
Published 6 June 2008
Online at http://www.njp.org/
doi:10.1088/1367-2630/10/6/065001

Abstract. When atoms are loaded into an optical lattice, the process of gradually turning on the lattice is almost adiabatic. In this paper, we investigate how the temperature changes when going from the gapless superfluid phase to the gapped Mott phase along isentropic lines. To do so we calculate the entropy in the single-band Bose–Hubbard model for various densities, interaction strengths and temperatures in one and two dimensions for homogeneous and trapped systems. Our theory is able to reproduce the experimentally observed visibilities and therefore strongly supports the view that current experiments remain in the quantum regime for the considered lattice depths with low temperatures and minimal heating.

[6] Author to whom any correspondence should be addressed.

Contents

1. Introduction **2**
2. Theoretical description **3**
3. Methods **4**
3.1. The canonical worm algorithm 5
3.2. Flat histogram methods 5
3.3. Thermodynamic integration 7
3.4. Numerical strategy 8
4. Isentropic lines in 1D systems **8**
4.1. Homogeneous system 9
4.2. Entropy distribution in a constant parabolic trapping potential 11
4.3. Entropy distribution in a realistic parabolic trapping potential 15
4.4. Tonks gas: 1D trapped case 18
5. Results in 2D **19**
5.1. Homogeneous 2D superfluid 19
5.2. The superfluid to Mott-insulating transition in a parabolic trap 21
6. Interpretation of experimental results **23**
6.1. Dependence of visibility on temperature and trapping potential 23
6.2. Comparison to experimental results 25
7. Summary **28**
8. Outlook and conclusions **29**
Acknowledgments **30**
References **30**

1. Introduction

During recent years, substantial progress has been made in cold atom experiments. Among the greatest achievements are the experimental realization of the superfluid to Mott-insulating transition with bosonic atoms in optical lattices [1] and the crossover between a Bose–Einstein condensate (BEC) and a Bardeen, Cooper and Schrieffer (BCS) superconducting state in fermionic quantum gases [2]. Due to the good tunability the excitement of using cold atomic gases as a so-called quantum simulator has been hard to temper. Such quantum simulators are systems which mimic—in a controllable and ultraclean way—simple strongly interacting models, such as the Hubbard model. With ultracold atom experiments the dream of using such quantum simulators to obtain new insight into the long-standing problems of other research areas seems 'almost' feasible. One of the notorious challenges of condensed matter physics that might be solved in such quantum simulations is the fermionic Hubbard model [3, 4], believed to be relevant for high-temperature superconductivity [5].

Beside the use as quantum simulators, the unprecedented tunability of cold atomic systems makes them very promising candidates for quantum computers. The experimental production of entanglement has been a large step forward into performing quantum computations [6].

The prerequisite of applying the quantum simulator to unknown physics, is a complete understanding of the present experiments. One would expect full agreement between the

current generation of bosonic experiments and theory, since the properties of the underlying homogeneous Bose–Hubbard model are rather well studied. However, our understanding of the present experiments is far from complete. The interpretation of the results is mainly complicated by two points:

(1) The presence of an external trapping potential can cause the spatial coexistence of the superfluid and Mott phases. This replaces the quantum phase transition by a gradual crossover, which can obscure the characteristic signal of the quantum phases.

(2) A change in temperature due to adiabatic or non-adiabatic origins can also hide the signature of the quantum phase transition, replacing it by a thermal transition. Considerable heating in current experiments would cast serious doubt [7]–[9] on former interpretations. Knowledge of the temperature in an optical lattice is therefore highly desirable, but whereas the temperature of a weakly interacting bosonic gas in a parabolic trap can be measured accurately, no reliable temperature measurement exists in the presence of a deep optical lattice.

In this paper, we re-examine the interpretation of recent experiments of bosons in optical lattices focusing on the effect of temperature in the presence of a trapping potential. We determine the lowest temperature that can be reached by loading the atoms adiabatically into the optical lattice. It is reasonable to assume that such processes are isolated and close to thermodynamic equilibrium at all times, since ramping up the lattice is typically slow ($\sim$16 ms per increase E_R in lattice laser intensity) compared to the tunneling rate of the bosons ($\sim$1 kHz, except for the deepest lattices) [10]. This assumption gives a lower bound for the temperature which can be achieved in the experiments without applying further cooling techniques.

We compare the results of our approach with the measured experimental interference patterns over the whole parameter range. In contrast to the previous works [7, 8, 11, 12], we can take the full range of realistic heights of the lattice potential and the full trapping potential into account and our calculations are approximation-free and based on first principles.

After introducing the theoretical description of the quantum gas in section 2, we discuss the quantum Monte Carlo (QMC) methods we developed in section 3. This section can be skipped by the non-expert. In section 4, we present results for the entropy in one dimension (1D). We compare homogeneous systems with systems in the presence of realistic trapping potentials across the superfluid to Mott-insulating transition and we also study the Tonks–Giradeau gas. We make contact with analytic approximations where possible, and we study the validity of the local density approximation (LDA). Section 5 is dedicated to the entropy in 2D homogeneous and trapped systems. We study the influence of the trapping potential, density, temperature, and of the actual experimental procedure on the visibility in section 6. We also compare the visibility obtained computationally with experimental data.

2. Theoretical description

In order to prepare ultracold atoms in an optical lattice, the atoms are confined in an external trapping potential and cooled till they BEC. Thereafter, additional lasers forming an optical lattice are turned on. One gradually increases the intensity of these lasers, slowly enough to remain in a low-energy state but also fast enough such that external influences are small.

Adiabaticity can be checked by reversing the process, i.e. decreasing the intensity and comparing the state at a certain lattice height shows the same experimental signature as the

corresponding state while switching on the lattice. Such experiments indicate that the loading of the atoms might to a good approximation be considered as adiabatic.

Atoms loaded in a sufficiently deep optical lattice are described by the Bose–Hubbard model [13],

$$H = -t \sum_{\langle i,j \rangle}^{L^d} b_i^\dagger b_j + \frac{U}{2} \sum_i^{L^d} n_i(n_i - 1) + \sum_i^{L^d} \epsilon_i n_i. \tag{1}$$

The notation $\langle i, j \rangle$ refers to the sum over nearest-neighbor sites only. Bosons are created on site j by the operator $b_j^\dagger$ and the number of bosons on site j is counted by the number operator n_j. The kinetic term describes hopping of the bosons with tunneling amplitude t, while the on-site repulsion has strength U. We will work in the canonical ensemble with a constant number of particles, N. The linear system size is L and we work in dimensions $d = 1$ and 2. We restrict ourselves to a single-band Bose–Hubbard model, which is sufficient at low temperatures and lattice intensities around the superfluid-Mott transition, but it becomes approximate for very low repulsion or high temperatures.

The external trapping potential is included using $\epsilon_i = v_c r^2$, where v_c describes the strength of the trapping and r the distance to the center of the lattice. If red detuned lasers are applied for creating the optical lattice potential the focusing of the lasers gives rise to an additional confinement. Under proper alignment of the two trapping potentials, the total trapping is given by $\epsilon(i) = m\omega^2 r^2/2$ [14] with

$$\omega^2 = \omega_0^2 + 8V_0/(mw^2), \tag{2}$$

where w is the waist of the lattice laser beam and V_0 its intensity expressed in single-photon recoil energies, $E_R = h^2/2m\lambda^2$. Here, λ is the wavelength of the lattice laser beam and m is the mass of the atoms. We took the waists isotropic and neglected corrections of the order of $\sqrt{V_0}$. The second term in equation (2) dominates already for moderately strong lattices.

The homogeneous Bose–Hubbard system shows a quantum phase transition from a superfluid to a Mott-insulating state when the filling is commensurate [15]. The transition occurs at $(U/t)_c = 3.28(4)$ [16, 17] in 1D systems, and at $(U/t)_c = 16.74(1)$ [18, 19] in 2D systems. Whereas in the superfluid state a continuous excitation spectrum exists at low energies, the Mott insulator is characterized by a gap just above its ground state.

Analytically the entropy in the Bose–Hubbard model has been studied for non-interacting [11, 20] and weakly interacting [11, 12] bosons. The strongly interacting limit for the Mott insulator and the Tonks regime have been considered for homogeneous [12, 20] and trapped systems [12, 21]. In 3D, the entropy deep in the superfluid and Mott insulating phases was calculated using effective masses [22]. Information on the trapped system was then obtained using the LDA. The Bose–Hubbard model can only be solved analytically in these limiting cases, where one is very deep in the superfluid or Mott-insulating phase. Close to the phase transition numerical tools have to be employed, such as the QMC simulations performed here.

3. Methods

In this section, we discuss a number of methods to determine the entropy

$$S(\beta) = \beta(E - F) = \beta E + \ln(Z), \tag{3}$$

where E is the total (internal) energy of the system, $\beta = 1/T$ the inverse temperature and $F = -\ln(Z)/\beta$ is the free energy. We use $k_B = 1$. The main challenge is an accurate calculation of the partition function. It turns out that a combination of two methods discussed below gives the best results. Both are accurate, and do not involve any fitting nor noisy derivatives of numerical data, but they are efficient in different temperature ranges. The results of both methods have been checked against each other for consistency. The flat histogram methods (section 3.2) work best at high temperatures, whereas the thermodynamic integration method (section 3.3) works better at low temperatures. This section is intended for the technically oriented readers and it is not necessary to read it in order to understand the discussion on the results in the next sections.

3.1. The canonical worm algorithm

All our simulations employ a canonical worm algorithm. A worm algorithm [23] in the path-integral representation is a QMC algorithm where the decomposition of the partition function,

$$Z = \mathrm{Tr} \sum_{n=0}^{\infty} \int_0^{\beta} \mathrm{d}t_n \int_0^{t_n} \mathrm{d}t_{n-1} \cdots \int_0^{t_2} \mathrm{d}t_1 \mathrm{e}^{-t_1 H_0} V \mathrm{e}^{-(t_2-t_1)H_0} \cdots \mathrm{e}^{-(t_n-t_{n-1})H_0} V \mathrm{e}^{-(\beta-t_n)H_0} \tag{4}$$

is sampled indirectly by making local moves in the Green function sector, which is the extended configuration space of world lines with two open ends. Simulating the Bose–Hubbard model, we choose as diagonal part H_0 the potential energy, whereas the hopping terms are the perturbation V.

In a canonical worm algorithm, the operators of the equal-time Green function $b_i(\tau)b_j^{\dagger}(\tau)$ are propagated simultaneously. The extended partition function we sample reads

$$\begin{aligned} Z_e &= \mathrm{Tr}\left[\mathcal{T}\left(\left(b_i(\tau)b_j^{\dagger}(\tau) + \mathrm{h.c.}\right)\exp(-\beta H)\right)\right] \\ &= \sum_{n=0}^{\infty} \sum_{\{|i_1\rangle\},\cdots,\{|i_{n+1}\rangle\}} \sum_{i,j} \int_0^{\beta} \int_0^{t_n} \cdots \int_0^{t_2} \cdots W_e(.)\mathrm{d}t_1 \cdots \mathrm{d}\tau \cdots \mathrm{d}t_n, \end{aligned} \tag{5}$$

where the terms $W_e(.)$ denote

$$\begin{aligned} W_e(.) = {} & \mathrm{e}^{-t_1 E_1}\langle i_1|V|i_2\rangle \mathrm{e}^{-(t_2-t_1)E_2} \cdots \mathrm{e}^{-(\tau-t_k)E_k}\langle i_k|b_i^{\dagger}(\tau)b_j(\tau)|i_{k+1}\rangle \\ & \times \mathrm{e}^{-(t_{k+1}-\tau)E_{k+1}} \cdots \mathrm{e}^{-(t_{n+1}-t_n)E_{n+1}}\langle i_{n+1}|V|i_1\rangle \mathrm{e}^{-(\beta-t_{n+1})E_1}, \end{aligned} \tag{6}$$

with $E_i = \langle i_1|H_0|i_1\rangle$, and we have introduced sums over a complete basis set between any two off-diagonal operators. The terms W_e are all positive and can thus be used as weights in a Monte Carlo sampling.

An efficient updating scheme has been presented in [24, 25] and allows the straightforward computation of the kinetic and potential energy, density, compressibility, equal-time Green function and superfluid density. However, the partition function is not a thermodynamic average and is harder to compute.

3.2. Flat histogram methods

The goal of a flat histogram method is to obtain a density of states $\rho(X)$ (where the coordinate X in classical simulations is usually the energy) directly by a random walk in X-space instead

of performing a canonical simulation at fixed temperature. By sampling each value of X with a probability $\mathcal{G}(X) \propto 1/\rho(X)$ we obtain a flat (constant) histogram $H(X)\rho(X)\mathcal{G}(X) = \text{const}$.

In the Wang–Landau sampling scheme [26], a crude guess for $\mathcal{G}(X)$ is iteratively updated until it converges by a multiplicative factor f. During consecutive Wang–Landau iterations, f is reduced according to $f \to \sqrt{f}$ when the current histogram $H(X)$ is considered to be sufficiently flat. Then the histogram is reset, we have a more accurate estimator for the density of states, and the sampling restarts with the smaller f. The convergence of the scheme was proven by Zhou and Bhatt [27]. In particular, they showed that the minimum number of steps in each Wang–Landau iteration should scale as $1/\sqrt{f}$. The generalization of the Wang–Landau scheme to quantum systems was discussed in [28]. Here, we generalize equation (4) of [28] to the path-integral formulation:

$$\begin{aligned} Z_\lambda &= \mathrm{Tr}\exp\left(-\beta\left(H_0 - \lambda V\right)\right) \\ &= \mathrm{Tr}\sum_{n=0}^{\infty}\int_0^\beta \mathrm{d}t_n \int_0^{t_n} \mathrm{d}t_{n-1}\cdots\int_0^{t_2} \mathrm{d}t_1 \mathrm{e}^{-t_1 H_0}\lambda V \mathrm{e}^{-(t_2-t_1)H_0}\cdots \mathrm{e}^{-(t_n-t_{n-1})H_0}\lambda V \mathrm{e}^{-(\beta-t_n)H_0} \\ &= \sum_{n=0}^{\infty} g(n)\lambda^n. \end{aligned} \tag{7}$$

The expansion order n corresponds to the number of kinks (particle hoppings) present in the path integral representation of a configuration. The original partition function (which is a function of the inverse temperature β) can be found back by setting $\lambda = 1$. The density of states $g(n)$ corresponds to

$$g(n) = \sum_{|i_1\rangle,\ldots,|i_n\rangle}\sum_{i,j}\int_0^\beta\int_0^{t_n}\cdots\int_0^{t_2} W(.)\mathrm{d}t_1\cdots\mathrm{d}t_n, \tag{8}$$

where W denotes the weight of a diagonal configuration,

$$W(.) = \mathrm{e}^{-t_1 E_1}\langle i_1|V|i_2\rangle \mathrm{e}^{-(t_2-t_1)E_2}\cdots \mathrm{e}^{-(t_n-t_{n-1})E_n}\langle i_n|V|i_1\rangle \mathrm{e}^{-(\beta-t_n)E_1}. \tag{9}$$

In such configurations all world-lines are continuous, and it occurs during the Monte Carlo run when the two open ends (worms) cancel each other on the same site and imaginary time.

Using the canonical worm algorithm [24, 25], the density of states can be obtained as follows: a single Monte Carlo step is defined from a diagonal to a new diagonal configuration and has an acceptance factor q'. Taking the density of states into account, the acceptance factor should be modified to

$$q(x \to y) = \min\left[1, g(x)q'/g(y)\right], \tag{10}$$

where $g(x)$ is the density of states corresponding to the expansion order of the old configuration x. When the expansion order of the new configuration is larger than a predefined maximum expansion order, the update is rejected.

When the Wang–Landau iteration is finished, we can obtain the partition function for all values of λ. For the Bose–Hubbard model that means that we obtain a whole set of partition functions through the scaling $\beta t \to \beta t\lambda$, $U/t \to U/\lambda t$ (thus βU is constant). A trap would also rescale as $V \to \lambda V$, which makes this scaling less useful in the trapped case and we use it just to obtain values at $\lambda = 1$. If we had worked in the grand-canonical ensemble, the chemical potential would scale analogously, and we lose all control over the particle number. Here, we see a distinct advantage of the canonical ensemble over the grand-canonical ensemble.

The normalization of $g(n)$ is fixed by calculating the partition function Z_N in the canonical ensemble for the case without hopping ($t = 0$).

3.3. Thermodynamic integration

The second method we discuss is the thermodynamic integration method. We choose a set of inverse temperatures

$$\beta_0 = 0 < \beta_1 < \beta_2 < \cdots < \beta_n. \tag{11}$$

Then, the partition function can be written as

$$\ln Z_{\beta_n} = \ln Z_0 + \sum_{j=1}^{n} \ln \frac{Z_{\beta_j}}{Z_{\beta_{j-1}}}. \tag{12}$$

The partition function at infinitely hot temperatures $Z_0 = Z_{\beta_0=0}$ can be found by solving the combinatorial problem of placing N bosons on L lattice sites,

$$\ln Z_0 = \ln \left(\begin{array}{c} L+N-1 \\ N \end{array} \right) = \sum_{j=L}^{L+N-1} \ln j - \sum_{j=1}^{N} \ln j. \tag{13}$$

The ratios in equation (12) can be estimated through the weights introduced in equation (5),

$$\begin{aligned} \frac{Z_{\beta_{j-1}}}{Z_{\beta_j}} &= \frac{\sum_\sigma W_{\beta_{j-1}}(\sigma)}{\sum_\sigma W_{\beta_j}(\sigma)} \\ &= \frac{\sum_\sigma \frac{W_{\beta_{j-1}}(\sigma)}{W_{\beta_j}(\sigma)} W_{\beta_j}(\sigma)}{\sum_\sigma W_{\beta_j}(\sigma)} \\ &= \left\langle \frac{W_{\beta_{j-1}}(\sigma)}{W_{\beta_j}(\sigma)} \right\rangle_{\beta_j}, \end{aligned} \tag{14}$$

where we sample all configurations σ at the temperature β_j. In the canonical worm algorithm, we have to measure

$$\begin{aligned} \frac{W_{\beta_{j-1}}(\sigma)}{W_{\beta_j}} &= \frac{\beta_{j-1}^n \mathrm{e}^{-\beta_{j-1} E_d}}{\beta_j^n \mathrm{e}^{-\beta_j E_d}} \\ &= \left(1 - \frac{\Delta\beta}{\beta_j}\right)^n \mathrm{e}^{\Delta\beta E_d}, \end{aligned} \tag{15}$$

with $\Delta\beta = \beta_j - \beta_{j-1}$ and E_d the time averaged potential energy of the configuration. We can thus compute the partition function at β_j if we know the partition function at β_{j-1}.

The accuracy of the scheme depends on the overlap between the system at β_j and the one at β_{j-1}. If the overlap is small, the error on the partition function will increase rapidly and propagate systematically on to lower temperatures. In particular, the first term β_1 should be chosen sufficiently close to zero, since there are only contributions if the expansion order is zero. The fluctuations in the (diagonal) energy in equation (15) are exponentially hard to control. We therefore choose our set of values of β such that $\Delta\beta E_d < 1$. At large values of U or large particle numbers, more β-points are required. When we are close to the ground state, things get easier since there energy fluctuations are suppressed. In the limit that $\Delta\beta$ is infinitely small, the scheme reduces to an energy integration. Note, however, that the scheme remains exact when $\Delta\beta$ is finite.

3.4. Numerical strategy

Although we tried a number of alternatives, none of them were satisfactory. We briefly make some remarks about them. We tried to use

$$\frac{\partial S}{\partial U} = -\frac{(1/2)\partial \sum_i \langle n_i(n_i-1)\rangle}{\partial T} \tag{16}$$

and integrate the density fluctuation with respect to inverse temperature, but the scatter of the data was much bigger than the trend-line, which made this approach prohibitive without an adequate fitting procedure. Integrating the specific heat

$$S(\beta) = \int_0^{1/\beta} c_V(T')/T' \mathrm{d}T', \tag{17}$$

after differentiating the fitted curve through the energy was used in [22, 29, 30]. However, the division by the temperature is misbehaving at low T and the specific heat computed via the fluctuation formula $c_V = \beta^2(\langle E^2\rangle - \langle E\rangle^2)$ is a quantity that converges slowly in the Monte Carlo simulation. We have also combined a grand-canonical directed loop algorithm in the path-integral representation [31] with a QWL reweighting scheme, though the fact that the Wang–Landau reweighting also changes the density, made this approach very cumbersome. A better attempt was developing a canonical directed-loop algorithm in the stochastic series expansion (SSE) [32] and combining it with the QWL reweighting scheme. This approach has the advantage that one obtains all temperatures down to the one corresponding to the pre-chosen cut-off length at once. The drawback is that in a SSE representation the large values of U are also sampled, requiring extremely large orders even for moderate temperatures.

We obtained the highest accuracy by combining the two methods outlined in detail above. For high temperatures, up to $\beta t \approx 0.5$, the combination of the canonical worm algorithm with the flat histogram (QWL) scheme is best and fast. For larger βt, and since we are interested in the entropy for a very large number of βt over a relatively small temperature range, thermodynamic integration is best. This method should only be used close to the ground state. Otherwise the fluctuations in equation (15) are hardly controllable which might lead to large systematic errors.

We compare the accuracy of both the methods for a homogeneous 1D system and for a trapped 2D system in tables 1 and 2, respectively. The data and the error bars shown in the tables do not reflect the full computational cost, since for the propagation method we need many more intermediate values of β which are not shown in the tables. Similarly, for high β the flat histogram method requires only a single Monte Carlo run, but the cost scales exponentially with β (and the number of particles).

4. Isentropic lines in 1D systems

We will start our discussion of the 1D case with a homogeneous lattice and compare our results with analytic results in limiting cases. We will then gradually make the discussion more realistic (and more complicated) by including the parabolic confinement. The first step is discussing the entropy in a system of constant quadratic trapping, $v_c/t = \text{const}$. The second step is the case of an external parabolic trapping potential which is further strengthened by the focus of the lattice laser beams as is currently done in most experiments. We will compute the entropy with these two confining potentials starting in the superfluid and going to the Mott insulator or the Tonks–Giradeau gas. We will also check the quality of a numerically based LDA and will find that in its regime of validity the speed-up in computing the entropy of trapped systems is considerable.

Table 1. Comparison between the flat histogram quantum Wang–Landau ('QWL') and direct integration ('chain') methods for a homogeneous 1D Bose–Hubbard system with $U/t = 2$ and $N = 45$.

βt	S_{QWL}	S_{chain}
0.5	44.2(2)	44.08(3)
1.0	28.1(2)	27.83(3)
1.5	19.0(3)	18.6(1)
2.0	13.6(4)	13.2(1)
3.0	7.9(4)	7.6(6)

Table 2. Comparison between the flat histogram ('QWL') and direct integration ('chain') methods for a trapped 2D Bose–Hubbard system with $U/t = 100$ and $v_c/t = 2.5$.

βt	S_{QWL}	S_{chain}
0.2	36.9(3)	36.7(2)
0.5	12.2(3)	12.1(2)
0.7	7.2(4)	7.4(4)
1.5	1.9(2)	2.0(4)

4.1. Homogeneous system

The dependence of the entropy on the temperature is closely related to the energy spectrum. Weakly interacting superfluid systems have a continuous energy spectrum. Therefore, the entropy rises continuously with temperature. The Mott insulating states have an energy gap just above the ground state and entropy is exponentially suppressed up to temperatures of the order of $k_{\mathrm{B}}T/U \approx 0.1$ [12, 20]. The bands of excited states above the gap lead to a finite entropy if temperature is high enough. Strongly interacting incommensurate systems also have gaps in the spectrum, but at substantially higher energies, signaled by a plateau in the entropy in figure 1.

The dependence of the entropy per site on the filling is shown in figure 2 for different interaction strengths at a moderately low temperature $\beta t = 2$. For weakly interacting systems ($U/t = 2$), the entropy reaches a maximum at half filling and decays monotonically for higher filling factors. Mott regions in strongly interacting systems ($U/t = 12$) appear as strong dips in figure 2, where the entropy is exponentially suppressed because the temperature is well below the gap. We also make a comparison with the atomic limit approximation, where only single particle–hole excitations are taken into account. The agreement with the Monte Carlo data is only qualitative, because this approximation misses higher order particle–hole excitations which are important for $U/t = 12$. This is also the reason that the approximation incorrectly predicts a symmetric curve around $n = 1$. The approximation is expected to work well near commensurability, but already for densities 0.9 and 1.1 the deviation from Monte Carlo is considerable.

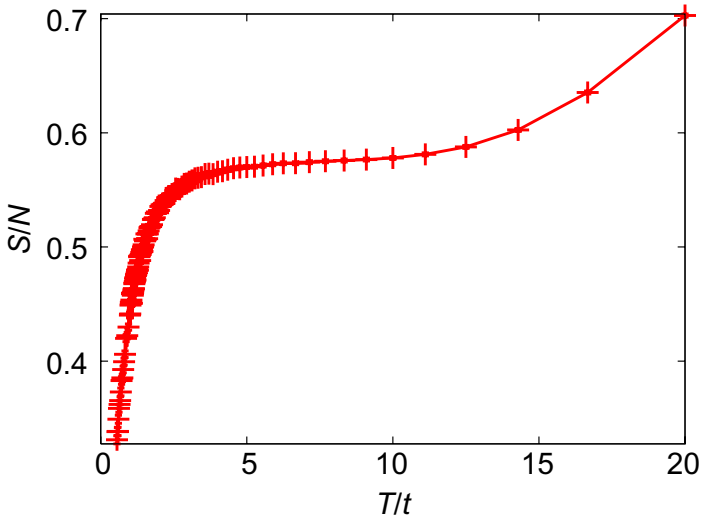

Figure 1. Entropy per particle as a function of temperature for a homogeneous 1D Bose–Hubbard system with $U/t = 100$, $N = 40$ and $L = 50$ ($n = 0.8$). The plateau hints at the existence of a gap in the excitation spectrum.

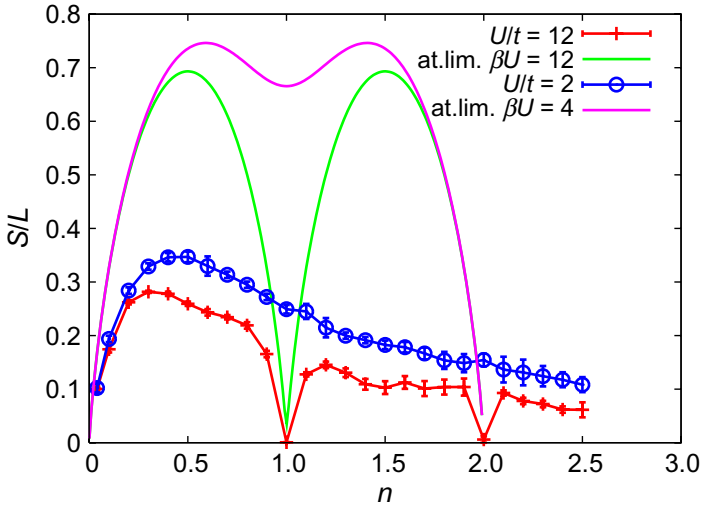

Figure 2. Entropy per site as a function of the filling factor for a homogeneous 1D Bose–Hubbard system. QMC data are shown by the symbols for $U/t = 12$ and $U/t = 2$ when $\beta t = 2$ and $L = 50$. The lines are guide to the eyes. Comparison is made with the atomic approximation at different temperatures where only particle–hole (1p–1h) contributions are taken into account.

Figure 3 shows the entropy per site for a system of 40 particles on a lattice of 50 sites as a function of the interaction strength U/t and inverse temperature $t/T = \beta t$. Since we are away from integer filling we are always in the superfluid phase. At intermediate and high temperatures $\beta t < 3$, the entropy decreases with increasing interaction strength. In contrast, at lower temperature, $\beta \gtrsim 3$, we see non-monotonic behavior of the entropy with a minimum close to the critical interaction strength in a commensurate system. The same qualitative behavior was

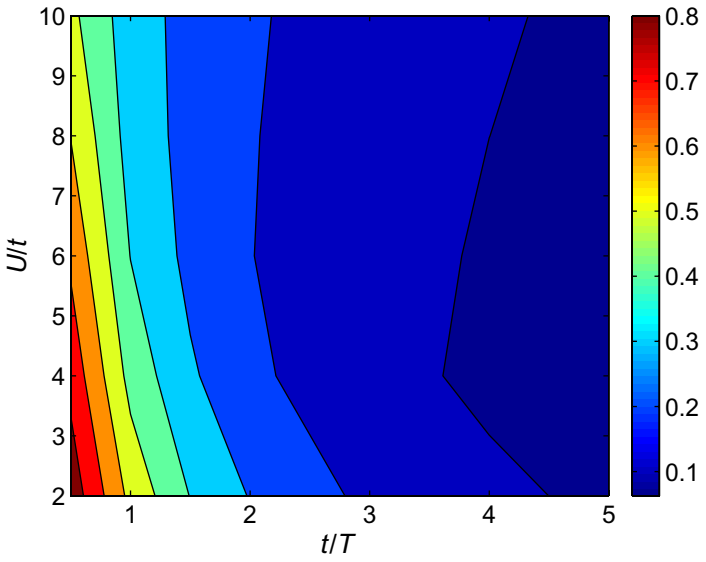

Figure 3. Entropy per site of a homogeneous 1D Bose–Hubbard model. There are 40 particles and 50 sites at incommensurate filling. The system is always in the superfluid regime. The error in the entropy is less than two percent in all cases. This representation of the entropy allows the final temperature to be read off easily when adiabatically ramping up the lattice. For instance, if the initial temperature is $\beta t = 2$ for $U/t = 2$, then the final temperature is $\beta t = 1.3$ for $U/t = 10$.

observed for a smaller lattice of $L = 20$ sites. The reason is the presence of the nearby quantum phase transition to a commensurate Mott state. The mass of the quasi-hole decreases when going away from the tip of the Mott lobe at $(U/t)_c$ to higher values of U/t. The quasi-hole absorbs more entropy and the entropy thus increases. Moving along isentropic lines we observe in units of t some mild heating when the initial temperature is reasonably high, $\beta t < 3$, but cooling if the initial temperature is sufficiently low, $\beta t > 4$.

The commensurate case in figure 4 shows the same behavior as figure 3 for low values of $U/t < (U/t)_c$ when we remain in the superfluid regime. However, when the Mott state develops, i.e. $U/t > (U/t)_c$, the gap in the spectrum opens and the entropy at constant temperature decreases considerably. Along adiabatic trajectories the temperature in units of t shoots up near the transition point. This has been discussed for the homogeneous system in [20], from which the authors deduced that the temperature in present experiments must be of the order of U. However, Rey *et al* [12] pointed out that in the presence of a parabolic confining potential less heating occurs in hard-core bosonic systems than in a homogeneous system. The next section addresses the same question for soft-core bosons.

4.2. Entropy distribution in a constant parabolic trapping potential

In the presence of an external trapping potential spatially separated quantum phases can coexist. In figure 5, we show two density profiles in the presence of a trapping potential. The first is for a superfluid state (figure 5(a)) in which the density closely follows the form of the trapping potential. The large local variance $\kappa = \langle n_i^2 \rangle - \langle n_i \rangle^2$ demonstrates the number fluctuations in the

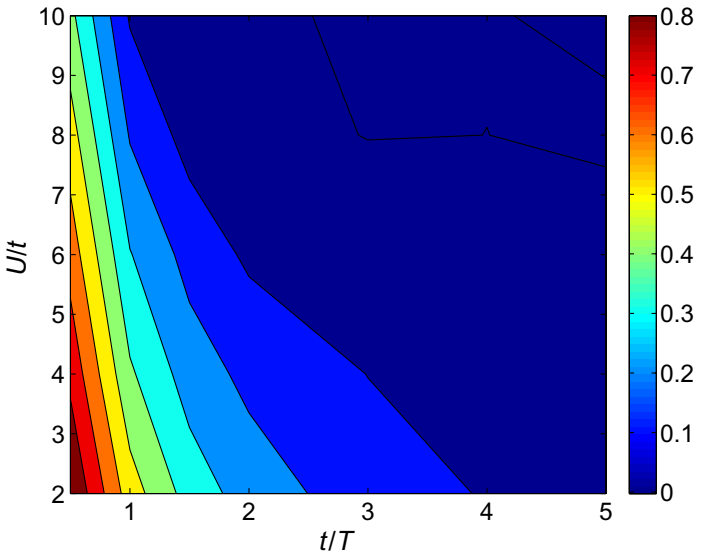

Figure 4. Entropy per site of a homogeneous 1D Bose–Hubbard model at commensurate filling. There are 50 particles and 50 sites. For $U/t > 3.28$ [16, 17] the system is in the superfluid phase in the thermodynamic limit at $T = 0$, for larger U/t a gapped Mott state is formed. The error in the entropy is of the order of 0.05, making it impossible to observe the exponential decay of the entropy in the Mott state.

superfluid state. The second density profile in figure 5(b) is for a state in which the central inhomogeneous region is surrounded by a Mott-insulating shell with commensurate filling and an outer incommensurate region. The variance shows a clear suppression of the density fluctuations in the Mott-insulating regions.

The coexistence of spatially separated quantum phases can be understood in terms of a site-dependent chemical potential, the so-called LDA. Physical quantities are determined by using on each site the results obtained for a homogeneous system with the corresponding chemical potential. The site-dependent effective chemical potential provides a scan through the phase diagram. This approximation has been shown to work nicely for such quantities as the density or the variance in regions where the trapping potential varies slowly [33, 34]. However, the LDA breaks down for steep trapping potentials and near the edges of Mott plateaus where numerical simulations are necessary to obtain reliable values [33]. To get a better understanding of the entropy distribution in an inhomogeneous system we developed a canonical and improved variant of the LDA, dubbed iLDA: we first calculate the exact density profile using a full QMC simulation for the trapped simulation. Then, we take for every site the entropy from a homogeneous run corresponding to that density. This variant has the advantage that we start from the exact density profile, taking into account the rounding near the edges of the Mott plateaus due to the finite gradient of the trap. We tested the approach by comparing the total entropy of the trapped system calculated as the sum of the single sites to full numerical simulations. We found, as shown in table 3, that the iLDA can capture the qualitative trend of full calculations, but cannot reproduce the exact values.

Using iLDA, we obtained the entropy profiles for the density profiles of figure 5. In a system where superfluid and Mott-insulating regions coexist, we clearly see that the Mott-like

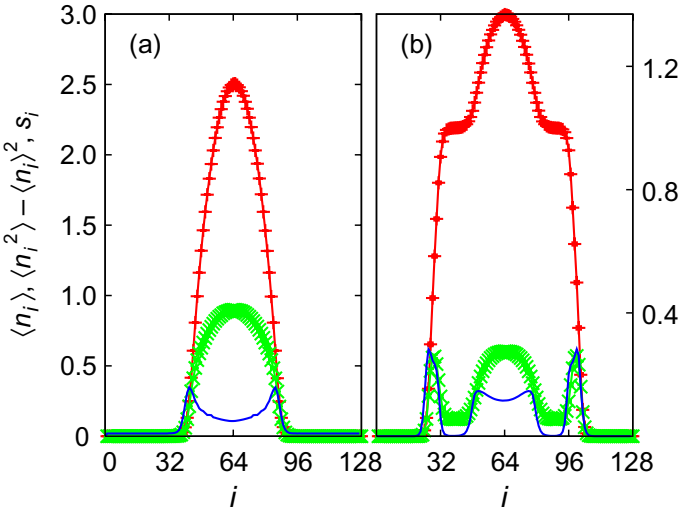

Figure 5. Density profile (red line, top curve in the center), density variance (green line, middle curve in the center) and entropy profile (blue line, lowest curve in the center) for a 1D trapped system for different parameters. (a) $U/t = 2$, inverse temperature $\beta t = 2$, system size $L = 128$, the trapping potential $v_c/t = 0.008\,29$ and the density $N = 80$. The total entropy calculated by the LDA approximation is $S_{\mathrm{LDA}} = 10.75$ and by QMC simulations $S_{\mathrm{QMC}} = 9.8(1)$. (b) $U/t = 12$, inverse temperature $\beta t = 2$, system size $L = 128$, the trapping potential $v_c/t = 0.008\,29$ and $N = 80$ particles. $S_{\mathrm{QMC}} = 9.2(1)$ from QMC and $S_{\mathrm{LDA}} = 8.3$ from LDA.

Table 3. Entropy comparison between iLDA and exact Monte Carlo results for different 1D system parameters. The trapping potential for the parameters in the third row is $v_c/t = 0.008\,29$.

Parameters	S by QMC	S by iLDA
Figure 5, left panel	9.8 ± 0.1	10.8
Figure 5, right panel	9.2 ± 0.1	8.3
$U/t = 6$, $\beta t = 1$, $N = 80$	22.7 ± 0.1	21.8
Figure 7, $U/t = 12$	7.9 ± 0.2	6.6

regions are not able to accommodate entropy and the whole entropy is in the superfluid regions. If the whole system is superfluid (figure 5(a)) the entropy varies only slowly from site to site and shows maxima at the filling close to $n \approx 1/2$. Since the filling is larger than one in the center a dip in the entropy profile develops.

In figure 6, we show the entropy calculated in a full QMC calculation for a constant trapping potential. In table 4, we show the values of temperatures following an isentropic line as extracted from the data. The concept of 'adiabatic heating' is complicated by the different energy scales (and units) used in the literature. It is important to define with respect to which energy scale the temperature is measured as illustrated in table 4. We see that along isentropic lines in the superfluid phase ($U/t < 10$) temperature in units of the hopping t remains roughly

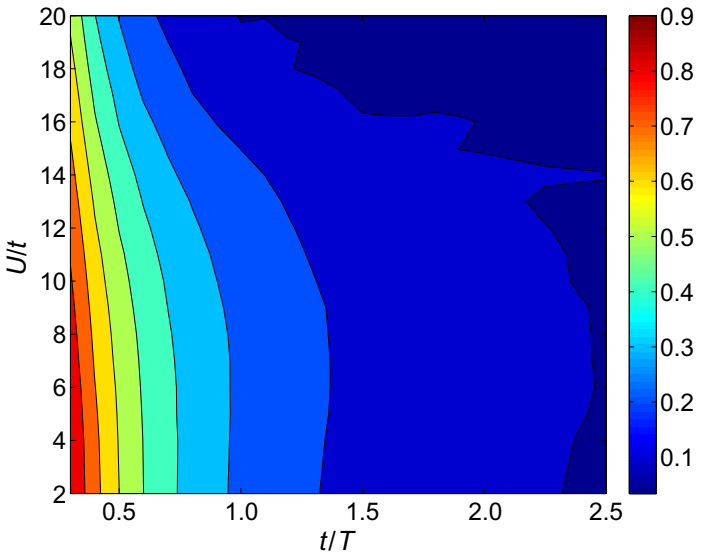

Figure 6. Entropy per particle of a 1D Bose–Hubbard model with constant trapping $v_c/t = 0.008\,29$. There are 80 particles and 128 sites. The magnitude of the errors is approximately 0.1–0.2. The roughness of the lowest isentropic line is within the error bars.

Table 4. Values of U/t, βt and $U\beta$ along an adiabatic line $S = 25$ for the same parameters as in figure 6. See figure 7 for the corresponding density profiles.

U/t	βt	βU
4	1.10(2)	4.4(1)
9	1.10(2)	9.9(2)
11	1.00(5)	11.0(5)
13	0.93(3)	12.1(4)
15	0.80(5)	12.0(8)
18	0.65(3)	11.7 (5)

constant. At higher temperatures there is some small heating in units of t, whereas at low temperatures we observe a little cooling.

This behavior can qualitatively be understood by looking at the density profiles along isentropic lines for different values of U/t, as shown in figure 7. Prior to the formation of a wide commensurate region, the temperature remains almost constant, for instance $\beta t = 1.1$ for $U/t = 4$ and $U/t = 9$ and $\beta t = 1.0$ for $U/t = 11$. Only when a considerable volume percentage of the system turns insulating the incommensurate edges cannot accommodate the entropy anymore which results in a rise in the temperature, i.e. $\beta t = 0.8$ for $U/t = 15$ to $\beta t = 0.7$ for $U/t = 20$. We checked that this effect is seen for a wide range of initial temperatures.

In units of the interaction strength U a cooling takes place. In particular, we see that for the chosen initial temperature the final temperature with respect to U stays below the temperature for which excitations in the Mott insulator are created in a homogeneous system. Therefore, the Mott insulator is stable up to the considered lattice height and the 'superfluid' regions take most of the excitations.

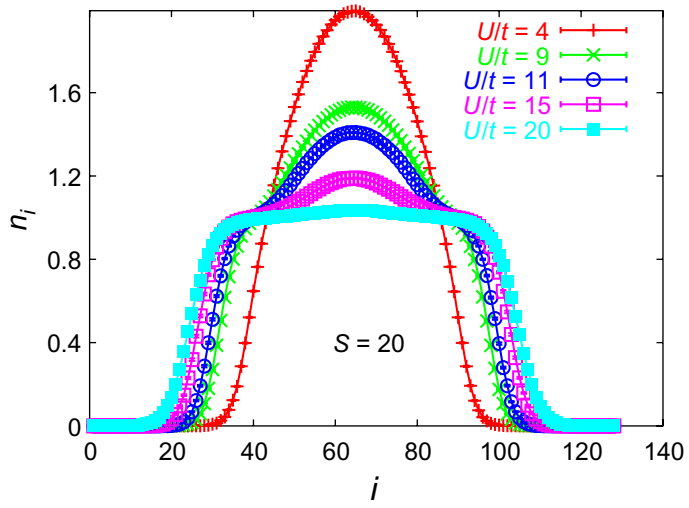

Figure 7. Density profiles along the isentropic line of $S = 20$ in figure 6. See table 4 for the corresponding temperatures.

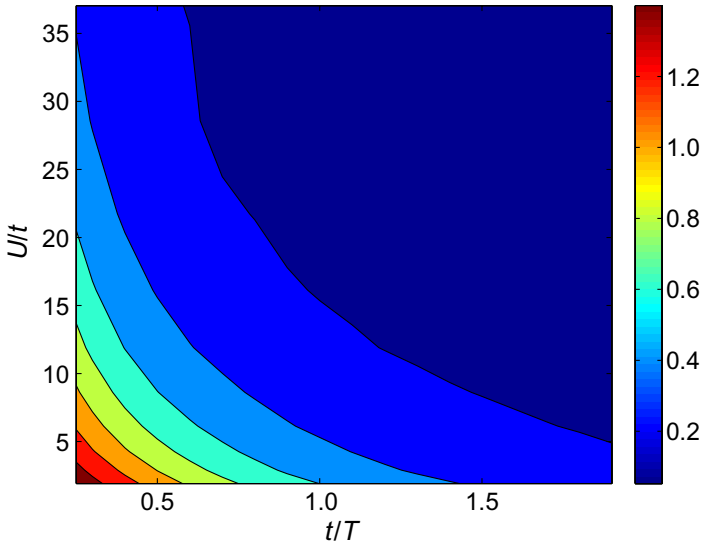

Figure 8. Entropy per particle of a 1D Bose–Hubbard model with varying trapping potential, taking the waist of the laser into account according to equation (2) with a magnetic trapping frequency $\omega_0 = 2\pi \times 30\,\mathrm{Hz}$ and a laser waist $w = 160\,\mu\mathrm{m}$ for ^{87}Rb atoms. Data points were calculated for $V_0 = 1, 2, \ldots, 10E_\mathrm{R}$ or for $U/t = 1.9, 2.9, 4.3, 6.1, 8.6, 11.9, 16.1, 21.7, 28.6$ and 37.0, and for $\Delta\beta t \sim 0.1$ or 0.2. There are 60 particles and 128 sites. The magnitude of the errors is a few percent.

4.3. Entropy distribution in a realistic parabolic trapping potential

Figure 8 shows the entropy when the finite waist of the optical lattice beam is taken into account (and v_c/t is no longer a constant but a function of the lattice-laser intensity). Table 5 gives the parameters for the temperature extracted along the isentropic line $S = 13$. We see that along this line the temperature in units of t increases whereas in units of U the temperature decreases.

Table 5. Values of U/t, βt and βU along an isentropic line $S = 13$ for the same parameters as in figure 8.

$V_0(E_R)$	U/t	v_c/t	βt	βU
4	6.13	0.008	1.62(4)	9.9(2)
5	8.62	0.011	1.35(4)	11.6(4)
6	11.90	0.015	1.10(4)	13.1(4)
8	21.74	0.028	0.70(4)	15.2(8)
9	28.57	0.037	0.61(2)	17.5(6)
10	37.04	0.049	0.49(2)	18.2(7)

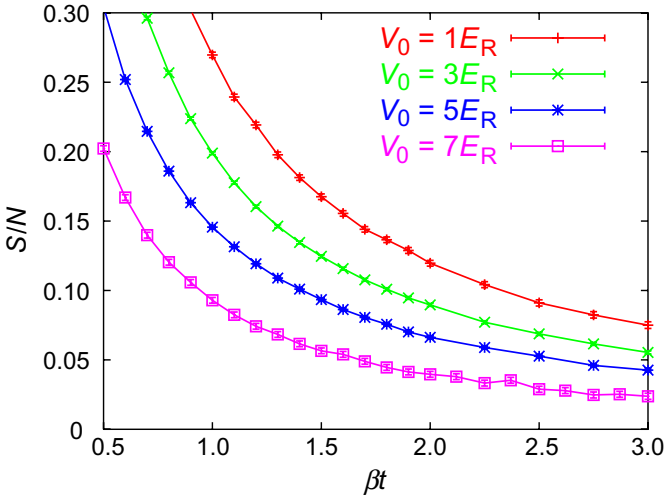

Figure 9. Entropy per particle as a function of the inverse temperature β for different intensities V_0 (expressed in recoil energies) of the lattice laser. The system has $N = 140$ particles on a lattice of $L = 128$ sites. We took a laser waist of $w = 160\,\mu$m. An isentropic line of $S = 10$ goes through $\beta = 3$ for $V_0 = 1$ and through $\beta = 1$ for $V_0 = 8$. See table 6 for temperatures along an adiabatic line $S = 20$.

This means that the formation of the Mott insulator is still possible starting at a low enough temperature, since the incommensurate regions take a lot of entropy.

Figure 9 shows the entropy as a function of the temperature for different strengths of the optical lattice potential. Compared to figure 8 the number of atoms is increased to $N = 140$. This has the consequences that even at low temperature only small Mott-insulating regions can form and an incommensurate region survives in the center of the trap (figure 10). In table 6, we show the temperature along the isentropic line $S = 20$. In units of t, we now get very strong heating, even in the superfluid phase, due to the high occupation which does not accommodate as much entropy as the low-occupation region (cf figure 2). However, in units of U we again find a temperature decrease.

One sees that the Mott insulator is stable against the temperature change, since the temperature stays below $0.1\,U$. Since the Mott-insulating regions are small and a broad

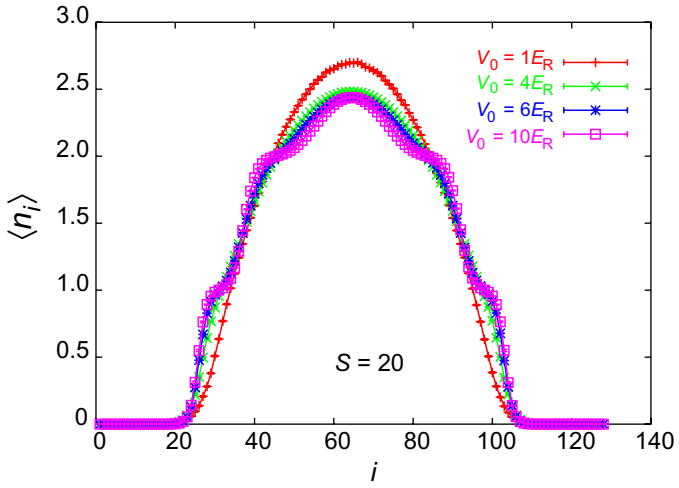

Figure 10. Density profiles along the isentropic line of $S = 20$ in figure 9. See table 6 for the corresponding temperatures.

Table 6. Values for U/t, βt and βU along an isentropic line $S \approx 20$ for the parameters as in figure 9. See figure 10 for the corresponding density profiles.

$V_0(E_R)$	U/t	$t\beta$	$U\beta$
1	1.92	1.70(2)	3.2(1)
4	6.13	1.15(5)	7.0(3)
5	8.62	1.00(3)	8.6(3)
6	11.90	0.85(5)	10.2(6)
7	16.13	0.70(2)	11.3(3)
8	21.74	0.55(4)	12.0(9)
9	28.57	0.46(2)	13.1(6)

Table 7. Values for U/t, βt and βU along an isentropic line $S \approx 50$ for the parameters as in figure 9.

$V_0(E_R)$	U/t	βt	βU
1	1.916	0.80(2)	1.5(1)
3	4.23	0.60(2)	2.5(1)
4	6.14	0.50(2)	3.1(1)
7	16.13	0.27(2)	4.4(5)
8	21.74	0.22(2)	4.8(4)

incommensurate region survives in the center, the Mott transition does not play a central role in the behavior of the entropy curves.

Starting at a higher initial temperature $\beta t = 0.8$ and following the isentropic line $S \approx 50$, the same qualitative effect of temperature increase in the units of t and decrease in the units of U can be seen in table 7. However, at $U/t \approx 20$, the temperature is still so high ($k_B T > 0.1\,U$) that no clean Mott-insulating region can be formed.

4.4. Tonks gas: 1D trapped case

When the potential energy between the atoms of a 1D Bose–Hubbard model increases, the particles behave more and more like hard-core bosons. The limit of infinite repulsion and no multiple occupancies of a site, is called the Tonks–Giradeau gas. Quantities such as the energy, average density, variance of the density can be computed accurately by assuming non-interacting fermions. Other quantities, such as the density matrix map to a non-interacting fermionic density matrix up to a phase factor coming from the Jordan–Wigner transformation. The experimental detection of the Tonks gas has demonstrated one of the fundamental concepts of quantum mechanics, namely, the absence of a clear meaning of statistics in 1D systems.

The Tonks regime has been observed with [21] and without a lattice [35]. In the experiment with a lattice, the data were analyzed using fermionization, and a good agreement with the experiment was found in the region $U/t > 5$. The fermionization results were obtained at different temperatures along adiabatic lines. Temperature rose from $\beta t = 2$ for a lattice depth of $V_0 = 4.6E_R$ to $\beta t = 0.77$ for $V_0 = 12E_R$ as a consequence of the change in v_c/t when ramping up the lattice. Consistently, it was argued in [7] that the temperature in the Tonks gas in a trap was of the order of the hopping t.

The Tonks problem was also studied by Monte Carlo simulations [36, 37] at a low but constant temperature $\beta t = 1$, which is of the same order as the one used in the fermionization approach. The authors compared hard-core and soft-core bosons for a homogeneous lattice and for constant trapping. They found a gradual crossover and found that the presence of a trap did not qualitatively change the Tonks onset.

The contrast in the experimental interference pattern was almost completely gone for the deepest lattices [21]. Although this is consistent with a strongly repulsive superfluid gas, one might fear that similar patterns are produced by either a Mott state or a thermal state due to a combination of soft-core bosons and an increased trapping depth.

Our analysis is again carried out in two steps. Firstly, we calculated the entropy of a 1D superfluid in the very low density limit trapped in a constant parabolic trap. Starting from a value $U/t \approx 5$, the system enters the strongly interacting regime, and we have seen that the temperature remains constant when further increasing the interaction. Thus, for a superfluid in the Tonks regime, adiabatic processes are (almost) isothermal when the external trapping is constant and weak.

Secondly, we make the simulation of the experiment more realistic. We numerically evaluate the Bose–Hubbard parameters using the tight-binding approximation, and obtain the same parameters U and t as in [36]. In contrast to [36], we now also calculate the trapping parameter v_c/t from the total axial trapping $\omega_{ax} = 2\pi \times 60$ Hz [21] for all optical lattice depths. We find in figure 11 some heating, even in the low-density superfluid phase. Along an adiabatic line similar to the one taken in [21], we find that the temperature increases from $\beta t = 2$ at $V_0 = 5E_R$ ($U/t = 6.9$) to $\beta t = 0.69$ at $V_0 = 12E_R$ ($U/t = 49.5$). Thus, the temperature increase compares very well to the one calculated assuming hard-core bosons [21].

Summarizing, we confirm that the experiment has indeed reached the gradual crossover toward the Tonks regime. The temperature remains of the order of the hopping t, even though a temperature increase of a factor of 3 is found due to the change in confinement strength v_c/t when ramping up the lattice. It is exactly this increase in temperature that prevents the Mott domains from developing, since for $V_0 = 12E_R$ ($U/t = 49.5$, $v_c/t = 0.073$) a broad Mott

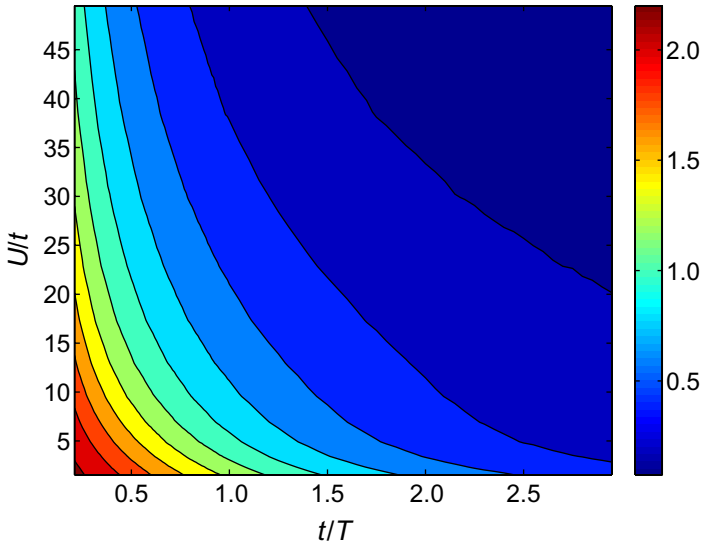

Figure 11. Entropy per particle of a 1D Bose–Hubbard model with changed trapping, approaching the Tonks regime for large values of U/t. There are $N = 15$ particles in the system of size $L = 50$.

domain appears in the center of the trap for 15 particles and $\beta t = 2$. At a temperature $\beta t = 0.69$ the central density is 0.9, however.

5. Results in 2D

5.1. Homogeneous 2D superfluid

We again start our analysis in 2D with the homogeneous case. The phase transition from the superfluid to the Mott phase occurs for a $n = 1$ commensurate system at $(U/t)_c = 16.74(1)$ [18, 19]. We calculate the entropy for a superfluid system close to commensurability, $n = 0.8$. In figure 12, the dependence of the entropy on the temperature and the interaction strength is shown. Its main behavior is similar to that in a 1D homogeneous case as reported in figure 1. At fixed interaction strength the entropy shows only a small increase for low temperatures. However, at a certain temperature it starts to increase strongly before it bends down again and a plateau is formed. This can, as in the 1D case, be related to the underlying band structure in which first excitations in the lowest band can be created. Above a certain temperature the corresponding gap in the energy band-structure causes an intermediate saturation before at even higher temperatures further bands can be excited.

As a function of the interaction strength, the entropy shows—for constant but low temperature—a minimum close to the superfluid to Mott insulator transition point of a commensurate system (inset of figure 12). As in the 1D case this can be attributed to the effective mass change of the quasi-hole which has its maximum close to the phase transition point for the homogeneous system.

The density fluctuation shown in figure 13 is consistent with the behavior of the entropy shown in figure 12, using the relationship of equation (16). For infinitely hot temperatures the density fluctuation is independent of U/t (not shown). For low values of U/t density

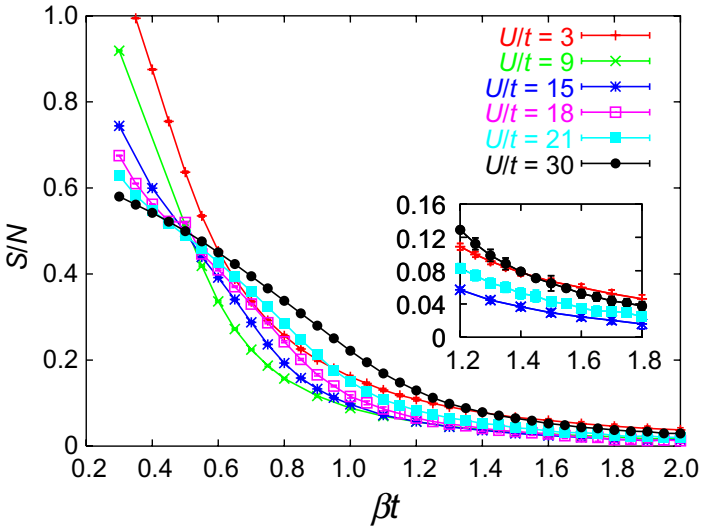

Figure 12. Entropy per particle for a system of size $L = 20 \times 20$ in the superfluid phase, $N = 320$. For a commensurate system, the transition happens at $(U/t)_c = 16.74(1)$ [18, 19]. For low temperatures, we see an initial heating with increasing U/t, but around the transition point the presence of the Mott phase is felt and the system starts to cool, thanks to the lower effective mass. For larger values of U/t, we see a further cooling for low temperatures since the Mott phase is far away and we go deeper inside the superfluid phase. The inset shows the entropy for low temperatures (same axes and symbols as in the main figure).

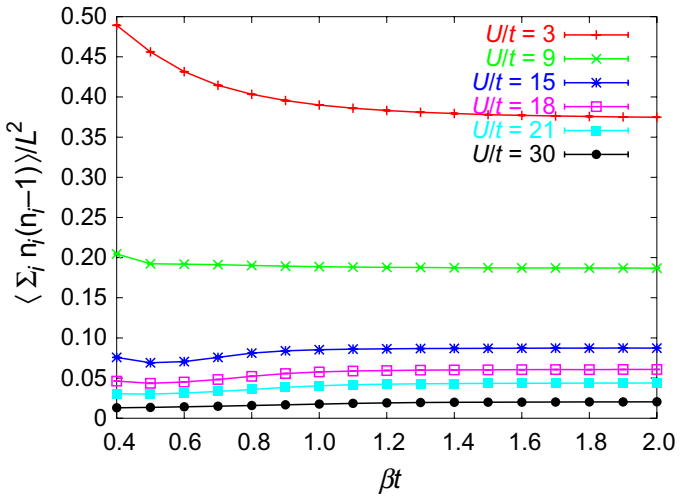

Figure 13. Density fluctuations for the same system as in figure 12. The curves bend down for low temperatures at low values of U/t. For large values of U/t a minimum is reached around $\beta t \approx 0.5$ while for larger values of βt the curves bend slightly upwards with temperature.

fluctuation goes down monotonically with βt. The normal–superfluid transition happens around $\beta t \approx 0.30(5)$ in our system of density 0.8 for a small lattice of 20×20 and $U/t = 3$. This transition belongs to the Kosterlitz–Thouless universality class, and was studied in detail for the commensurate case in [18, 19].

Table 8. Bose–Hubbard parameters chosen in the 2D trapped system.

U/t	5	10	15	20	25	50	100
v_c/t	0.2	0.33	0.47	0.61	0.74	1.11	2.50

For large values of U/t, we enter the quantum (thermal) critical regime determined by the quantum critical point $U/t = 16.74$ [18, 19] and a minimum in the density fluctuations is reached. This is clearly seen for $U/t = 15$ around $\beta t = 0.5$. For larger values of U/t, the minimum is reached at lower values of β. After this minimum is reached, the density fluctuations go slightly up with βt. The increase in the density fluctuations can be understood from the tendency of a dilute gas of vacancies (with respect to the $n = 1$ Mott state as a vacuum) trying to condense. In our canonical simulation, we will observe a tendency to increase the number of vacancies which will enhance pair formation. Thus, theoretically the density fluctuations contain a lot of information about the system, but from the practical point of view the almost flat slopes in the quantum regime make this quantity a bad candidate for thermometry.

5.2. The superfluid to Mott-insulating transition in a parabolic trap

In 2D, we only consider trapping potentials taking into account the influence of the finite waist of the lattice laser on our sample. We use the parameters shown in table 8. There are $N = 200$ bosons and the total system size is $L = 20 \times 20$. These parameters are a compromise between increasing the trapping frequency while still obtaining meaningful results on a lattice of size $L = 20 \times 20$. The filling in the system with $N = 200$ atoms for weak interactions is chosen such that it is close to $n = 2$ in the center for large U/t.

The entropy dependence on temperature is shown in figure 14 for different values of U/t. For low values of the temperature the slope for the curves is very flat. For higher temperature a clear increase in the entropy in the system can be seen. For low temperature the curves for different U/t almost coincide and only the curve for very strong interactions, i.e. $U/t = 100$, shows a considerably lower value of the entropy.

The behavior of the entropy can be explained by considering the density profiles of the system, shown in figure 15 along an adiabatic line $S = 10$. By increasing the optical lattice potential the central density goes down and we see the appearance of the $n = 1$ Mott-insulating region at $U/t \approx 25$. For stronger interactions, $U/t \sim 50$, small Mott-insulating regions with $n = 1$ and $n = 2$ exist. For $U/t = 70$, the Mott-insulating regions already cover a large volume fraction of the system as clearly signaled in the variance profile (not shown). The formation of the large Mott-insulating region causes the value of the entropy for the curve at $U/t = 100$ to lie below the others at low temperature.

The temperature evolution along isentropic lines for different initial temperatures is shown more quantitatively in table 9. When starting from a low temperature, we see almost no heating in units of t up to $U/t = 70$. The initially low entropy can be distributed over the remaining superfluid regions. Measuring the temperature in units of U leads to a cooling of the system below the value of $U/t = 70$. In contrast, for interaction strengths larger than $U/t = 70$ almost the whole system is occupied by a commensurate region and the incommensurate regions have a negligible volume fraction. The energy cost to generate an excitation in this situation corresponds in the bulk to large interaction energy and at the boundaries to large potential

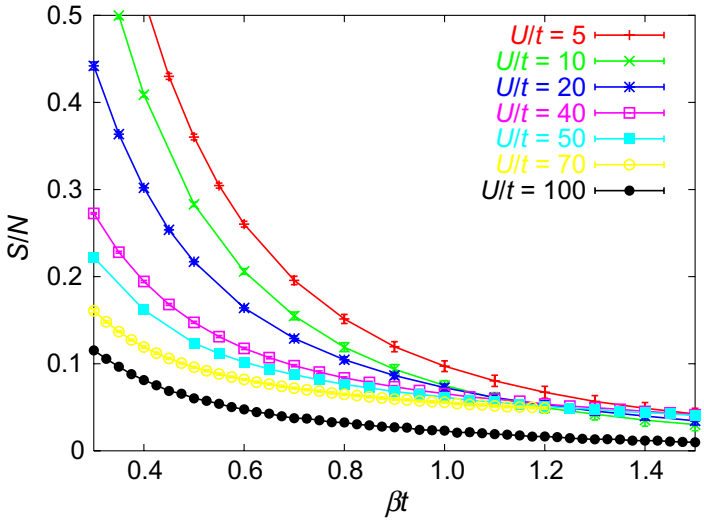

Figure 14. Entropy per particle as a function of inverse temperature for a set of different values of U/t with a trapping potential according to table 8. The curves for the intermediate curves coalesce within error bars for $\beta t > 1.5$. The curve for $U/t = 100$ is significantly below the other curves (see, however, the text) up to temperatures of the order $\beta t = 2$.

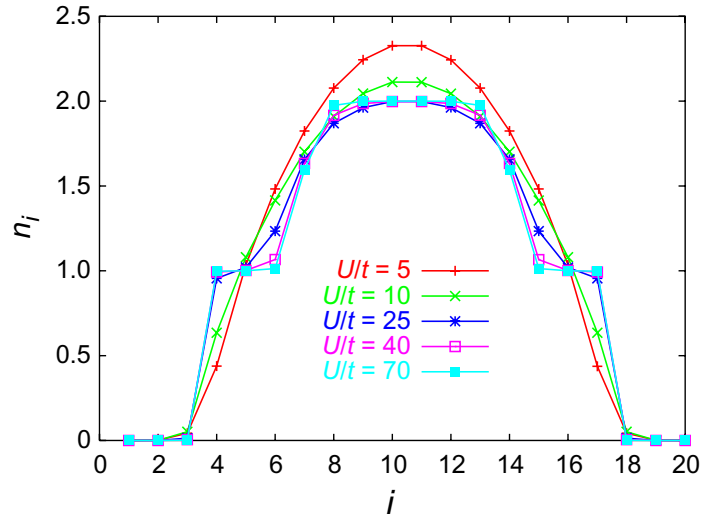

Figure 15. 1D cut of the density profiles for $y = L/2$ depending on the x-coordinate (labeled with 'i') along an adiabatic line $S = 10$. Error bars are smaller than the point size. See table 8 for the corresponding values of the trapping potential and table 9 for the corresponding temperatures.

energy cost resulting from the steep trapping potential. Hence, the entropy cannot be well accommodated in the system and the temperature in units of t increases more strongly than before when going to $U/t = 100$. In units of U, the temperature first drops before it increases again or saturates for large U/t lattice potential.

Table 9. Temperature along three adiabatic lines for the 2D trapped Bose–Hubbard model with parameters according to table 8.

U/t	$\beta_{S=10}t$	$\beta_{S=10}U$	$\beta_{S=40}t$	$\beta_{S=40}U$	$\beta_{S=300}t$	$\beta_{S=300}U$
5	1.40(5)	7	0.70(2)	3.5	0.13(1)	0.65
10	1.20(5)	12	0.60(2)	6	0.08(1)	0.8
25	1.30(5)	32	0.50(2)	12.5	0.06(1)	1.5
40	1.25(5)	50	0.40(2)	16	0.06(1)	2.4
50	1.20(5)	60	0.35(5)	17.5	0.06(1)	3
70	1.18(2)	83	0.25(1)	17.5	0.03(1)	2.1
100	0.58(3)	58	0.18(2)	18	0.01(1)	1

Starting with a low temperature ensures that the temperature remains low enough for the presence of the Mott-insulating regions. In contrast, when starting from a hot temperature (the right-most example in table 9 is already in the normal state), there is heating in units of t and only weak cooling in units of U. The quantum degeneracy regime is never reached. Note that the description by the one-band Hubbard model breaks down at such high temperatures.

6. Interpretation of experimental results

One of the standard experimental observation techniques consists of suddenly switching off the confinement and taking absorption images of the freely expanding gas after a finite flight time. The hereby resulting interference pattern is a reflection of the initial momentum distribution,

$$n\left(\vec{k}\right) = \left|w\left(\vec{k}\right)\right|^2 \sum_{i,j} \langle b_i^\dagger b_j \rangle \mathrm{e}^{\mathrm{i}\vec{k}\cdot(\vec{r}_i - \vec{r}_j)}, \tag{18}$$

where the factor $w(\vec{k})$ is the Fourier transform of the Wannier function [13]. The use of the momentum profiles (and also of the visibilities) has been subject to debate, since in this quantity different effects such as heating or the loss of coherence by stronger interactions have the same consequence. Furthermore, it is very difficult to extract information on the superfluid–Mott insulator transition point from these measurements in a trapping potential [16, 33, 38]. This is due to the spatially coexisting regions of superfluid and Mott-insulating character. A local measurement has to be implemented to obtain detailed information about the system. A first step in this direction has been taken by Fölling *et al* [39] who measured the density in thin slices. Experimental progress was reported for a local measurement of the density in http://physics.harvard.edu/∼greiner/newexp.html, and another proposal was made in [40]. Such measurement techniques should be preferred over the visibility, which is only well suited for identifying the Mott and superfluid phases far away from the transition point. In figure 15, we show the typical evolution of the density profiles (with Mott plateaus for strongly repulsive systems) along isentropic lines.

6.1. Dependence of visibility on temperature and trapping potential

Before we compare our results to the experimentally extracted quantities, we would like to point out some features of the momentum distribution in a trapped system at finite temperature.

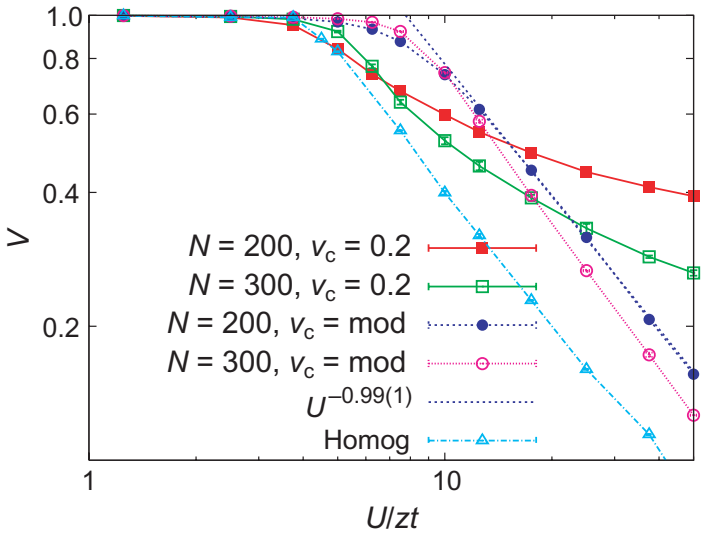

Figure 16. The role of the trap and the density on the visibility. We plot the visibility for a 2D system $L = 20 \times 20$ as a function of U/zt at a high temperature of $\beta t = 0.4$ for different fillings ($N = 200$ and 300) and trapping potentials. z is the coordination number. By $vc = 0.2$ we mean constant trapping $v_c/t = \text{const}$, while $vc = \text{mod}$ has parameters according to table 8. The dashed line ('$U^{-0.99(1)}$') is a power-law fit with exponent -1 within error bars. Comparison with the homogeneous system at the same temperature and on a lattice of the same size is made ('Homog'). Its slope is equally -1.

To do so we define the visibility V

$$V = \frac{n_{\max} - n_{\min}}{n_{\max} + n_{\min}}, \tag{19}$$

where $n_{\min}$ and $n_{\max}$ are the values of the largest and smallest value of $n(\vec{k})$.

Deep in the superfluid phase the darkest spot has almost $n_{\min} \approx 0$, leading to a visibility close to unity, while in the Mott-insulating phase the contrast between the brightest and the darkest spot is almost zero and one expects a very low visibility.

In figure 16, we show the visibilities for a trapped 2D Bose–Hubbard model at different densities. The calculation was done at a rather high temperature $\beta t = 0.4$. Even at this temperature regions with integer density and reduced compressibility exist. Precursors of the Mott-insulating regions can be seen in the density distribution and its variance around $U/t \sim 25$. Looking first at the case of a constant trapping potential, we see that for the chosen number of particles a higher density leads to a higher visibility at low U/t. The visibility is lower at high U/t since the Mott region is larger. Taking the steepening of the trap into account, we see that at low values of U/t the visibility is higher than that obtained with constant trapping for the considered particle number. The reason is the increased number of particles with density between one and two which form a superfluid edge between $n = 1$ and 2 Mott regions. The $n = 2$ Mott region is absent in the calculation with the constant trapping potential. For the two curves labeled 'vc = mod' taking the change in the trapping potential into account, the visibility is well fitted by a logarithmic curve for large values of $U/zt > 10$ in agreement with the finding

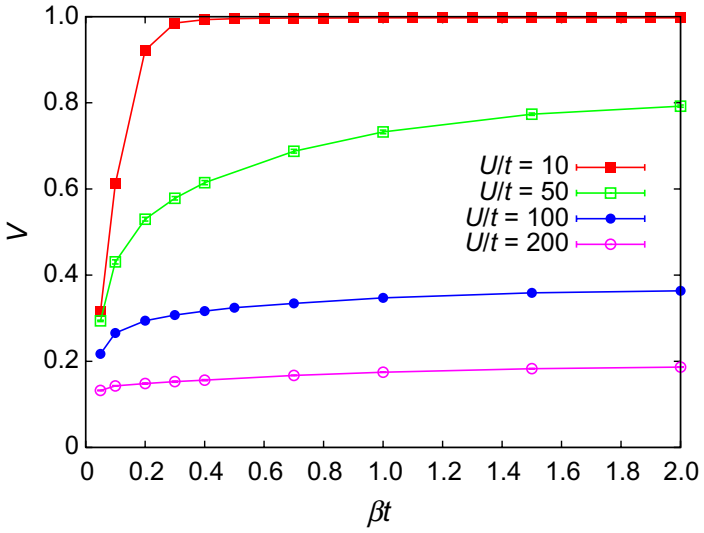

Figure 17. Temperature dependence of the visibility. We plot the visibility for a 2D system $L = 20 \times 20$ as a function of βt at constant particle number $N = 200$ for different values of U/t and v_c/t according to table 8.

in [41]. The reason for this good agreement might be the suppression of the volume fraction of the superfluid regions, such that only the Mott-insulating regions contribute to the decay of the visibility.

In figure 17, we show the visibility as a function of the inverse temperature for different strengths of the optical lattice potential. We see a strong decrease in the visibility if the temperature becomes of the order of $\beta t \approx 0.2$ when the quantum regime is left. A comparable decrease in the visibility at low temperature by changing the interaction strength is only possible when it is very large, i.e. $U/t = 200$ leads to a visibility of the order of 0.2. However, we should note that at high temperatures the single-band approximation of equation (1) loses its validity.

We further show the visibility along different isentropic lines in figure 18 for the same parameters as taken in table 9. The curves with low entropy (low-initial temperature) both have a slope of approximately -1, but the onset value U/t is different. Even for the curve with high entropy, corresponding to an initial normal state, the data points for large value of U/t seem to be consistent with this slope, but differ for a small value of U/t (experiments show a constant visibility within error bars at low values of U/t).

6.2. Comparison to experimental results

We will now take the trap and the isentropic temperature change into account, and compare with experiments. This is the hitherto most realistic description done without numerical approximations, but for the 2D case we fail to take the same number of atoms and system sizes as in the experiment. Further we ignore time-of-flight collision effects.

We first compare our 2D calculations to the experimentally obtained visibilities. Up to now we have evaluated the visibility using $n(\vec{k})$ at specific wave vectors $\vec{k}$. In experiments instead an average over a square around the brightest and darkest spot is taken (see [10] for the exact experimental procedure). The size of the area is a trade-off between the signal and noise.

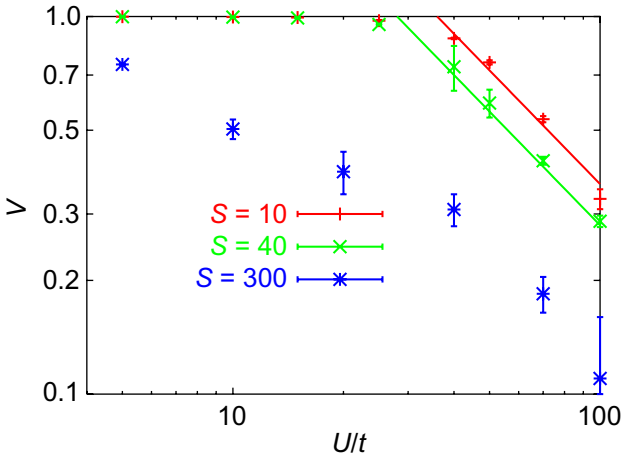

Figure 18. Influence of the initial temperature (via the entropy) on the visibility. We plot the visibility along the entropic lines of table 9. The visibility is computed by taking the brightest and darkest points of the momentum distribution of the Bose–Hubbard model only. The straight lines are fits with slope -1.

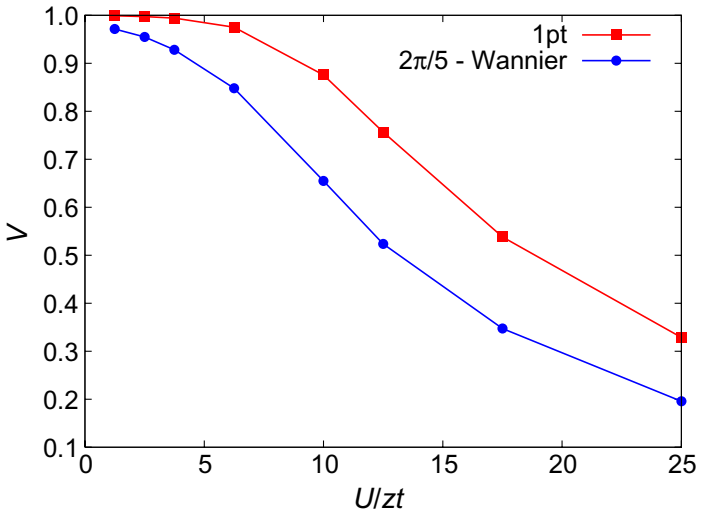

Figure 19. Effect of the experimental procedure on the visibility. We plot the visibility V as a function of U/zt along an isentropic line $S = 10$ with the same parameters as in figure 14 (see table 8). We compare the ideal theoretical value obtained by taking just the maximum and minimum in the momentum profile ('1pt') with the visibility after averaging over a square of length $2\pi/5$ taking the Wannier momentum profiles into account ('$2\pi/5$ - Wannier'). The error bars are smaller than the point size.

The squares are chosen such that the contribution of the envelope of the Wannier functions (cf equation (18)) is minimal, but not negligible. In figure 19, we show the different curves including the average and our previous definition of the visibility. For low values of the lattice height the curves without the Wannier envelope have values very close to one, whereas the curve

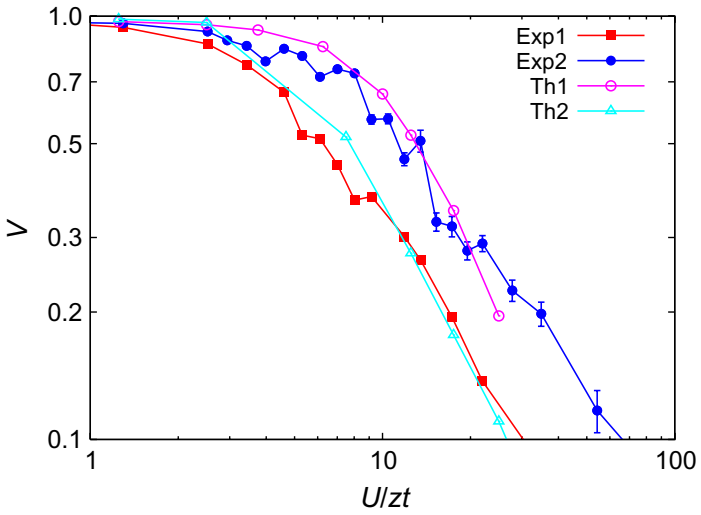

Figure 20. Comparison between the 3D data of [10] (blue and red) and the visibility found in our model (labeled 'Th1' and 'Th2'). The red data points have approximately 79 000 particles and the blue ones 224 000. This would correspond in the atomic limit to the presence of a small $n = 2$ plateau for the lower particle number and to a $n = 2$ plateau with almost half the number of particles for the higher number of particles [46].) Other experimental data fall in between these two curves, forming a 'band' with slope -1. The curve 'Th1' corresponds to the same parameters as in figure 14 along the adiabatic line $S = 10$. The theoretical data are treated in the same way as explained in the text by taking the Wannier functions and averaging over a square of size $2\pi/5$. The curve 'Th2' is a theoretical curve computed in the same way as 'Th1' and for the same system along an isentropic line $S = 5$ but for $N = 50$ particles such that the maximum occupation in the center of the trap does not exceed unity.

considering the Wannier envelope starts at a smaller value for the visibility. Fitting the slopes of the visibility with a power law gives roughly the same exponent for the theoretical and the experimental procedures, but the quality of the fit is better for the theoretical procedure.

Looking at the 3D experimental data, many groups find a visibility close to unity until $U/zt \sim 6.5$, where z denotes the coordination number. For larger values of U/t the decrease in visibility is well approximated by $V \sim (U/zt)^{\nu}$. The Zürich group [42, 43] finds $\nu = -1.36(5)$, whereas the Mainz group [44] finds $\nu \sim -0.98(7)$. The reason for the discrepancy is not fully understood. Similarly, the momentum distribution data on a log–log plot of the 2D system studied in [45] were consistent with a behavior of (t/U) and thus with a $\nu \approx -1$.

In figure 20, we show a comparison between our theoretical results for a 2D system and an example of the experimental data [44] taken for a 3D system. We rescale the interaction strength by the coordination number taking the mean-field effect between the different dimensions into account. We compare two theoretical curves with $N = 50$ and 200 particles. In the strong interaction limit, this corresponds to a density profile which has an $n = 1$ plateau for $N = 50$ and a profile with $n = 1$ and 2 plateaus for $N = 200$. The initial temperatures at $U/t = 5$ are $\beta t = 1.7$ and 1.4, respectively. Note that the particle numbers and temperature do not directly correspond to the experimental ones. For a direct comparison of an experimental to a theoretical

curve, 3D simulation with realistic particle numbers would be needed. However, we find good agreement in figure 20 of the theoretical visibility treated in the way described above with the experimental data even up to relatively strong optical lattices. This shows that the experimental visibility can be explained by just taking the isentropic change of the temperature into account. In particular, the system does not have to leave the quantum regime to reach the low values of the visibility. The drop in the visibility can be explained by the formation of a broad Mott-insulating region (cf figure 15). However, one sees that the visibility is not a very sensitive probe, since it does not distinguish between 2D and 3D data.

In 1D systems, the procedure to get a quantity similar to the visibility has to be changed, since the interference pattern consists of stripes. In [42], the superfluid to Mott-insulating transition in 1D tubes was considered. The experimentalists extracted the coherent fraction of the atoms by taking the ratio of the content in the interference peaks and the background. We compared (not shown) the experimental data with the theoretical calculations where we treated the results for the momentum distribution in the same way. We found the same order of magnitude and the same qualitative trends (e.g. the visibility for low-lattice heights is between 0.5 and 0.6 in both cases). A detailed comparison, however, is hindered by the presence of many different parallel tubes in the experiments and by the large uncertainties stemming from the difficulty of fitting the very sharp interference peaks.

7. Summary

An interpretation of experimental results on the superfluid to Mott-insulator transition taking finite temperature effects into account has been given before by several authors, with differing conclusions. We have addressed the possibility of adiabatic temperature changes when ramping up the lattice for the Bose–Hubbard model using unbiased and first-principle quantum Monte Carlo simulations. We find that the expressions ‘heating’ and ‘cooling’ have to be taken with care, since they strongly depend on the unit in which temperature is measured.

For the homogeneous case, we found some small heating in units of t near commensurability in the superfluid phase for high temperatures $\beta t < 0.5$. For low temperatures, there is some small heating for low values of $U/t < (U/t)_c$, but the system cools slightly for larger values of U/t when we are in the proximity of commensurability. At very low densities, temperature remains almost constant in the superfluid phase. When the density is commensurate, the temperature shoots up dramatically in units of t when the Mott gap opens in order to keep the accessible number of levels constant. This is in agreement with the findings of the previous studies [7, 12, 20].

In a trapped system, however, the situation is different as already noted in [12] for hard-core bosons. We find that in a 1D and a 2D system in a trapping potential the main entropy contribution comes from incommensurate regions with low filling $n \approx 0.5$. This is in good agreement with the finding for a 3D system of the Amherst group where they find that the non-commensurate edges between the Mott plateaus become normal and accommodate the entropy [22]. We found that the temperature increased in units of t when the size of the commensurate regions is broader than several lattice sites in the case of constant trapping. For realistic trapping and densities around one or two, we found a temperature increase in units of t, even in the weakly interacting regime. However, in units of U temperature decreases or saturates, and its value lies deep in the quantum regime for the commensurate regions. Only if the incommensurate regions around filling $n \approx 0.5$ are almost totally suppressed has the

entropy to be taken by excitations in the commensurate regions or regions with higher filling, by which the Mott-insulating regions might be destroyed. Our result is in agreement with the results of Gerbier who finds that current experiments easily reach the thermal insulator regime ($T < T^* \approx 0.2\,U$, where Mott-like features persist but superfluidity is absent), and possibly the quantum region [47]. In contrast to the predictions of [8], we find that for realistic parameters no runaway temperature occurs.

Assuming adiabaticity in current experiments is in agreement with theory remaining in the quantum regime. In particular, the drop in the visibility of the interference pattern can be fully explained within this framework and no additional temperature rise has to be taken into account.

Future experiments using the spatially resolved measurements of the density and higher order correlations will be able to confirm the creation of Mott-insulating regions as the first evidence was reported in [48]. Unfortunately, we have seen that the integrated density fluctuations are not very sensitive to temperature changes when one is deep in the quantum regime.

8. Outlook and conclusions

Our principal assumption that the loading of the lattice is approximately adiabatic needs to be verified considering the dynamical process at finite temperature. It will be equally important to extend our investigations to different and larger systems. A major goal will be to treat the full 3D Bose–Hubbard system with a realistic number of particles. Systems with different types of particles will have to be addressed as well, since the development of a new energy scale that does not scale with U will have a negative influence on the possibility of reaching the ground state adiabatically. The visibility results of theory [49] at low temperature and experiment [43, 50] are in disagreement for Bose–Fermi mixtures. It was believed that temperature is such that these systems are not in their ground state [49], and a study by Cramer *et al* [51] hints at heating effects for a weak inter-species coupling. Anti-ferromagnetism and entropy were previously addressed for a homogeneous Fermi–Fermi system in [30, 52, 53].

This work was motivated by the strongly different opinions that existed about temperature effects in the Bose–Hubbard model, ranging from a constant temperature to a runaway temperature. We have addressed this discussion in homogeneous and trapped, 1D and 2D Bose–Hubbard systems and the results of our work are uni-vocal: compatibility of experimental with numerical visibility curves (and density profiles) supports that the experimental initial temperature of the BEC is deeply in the superfluid phase, and that the quantum regime is not left when adiabatically ramping up the optical lattice, even in the presence of a considerable Mott domain. The temperature scales almost linearly with U when the Mott domain is considerable in size, but temperature remains a very low fraction of the value of U. We have copied the experimental procedure of measuring the visibility in our simulations and found good agreement. It turns out that the Wannier function and the averaging over a small region of the interference pattern produce an almost constant shift of the visibility as a function of U/t. For deep lattices, the trapping potential becomes effectively steeper, and different Mott plateaus are forced to form. The main contributions to the visibility come from particle–hole excitations giving the visibility a slope of -1 as a function of U/t. The superfluid volume fraction is too low, but it still absorbs most of the entropy, as we could infer from the LDA. Our results strongly support that experimentalists have observed the superfluid and Mott phases and their crossover in a trapped system.

Acknowledgments

We thank I Bloch, T Esslinger, A Georges, T L Ho, S Huber, H Moritz, J V Porto and S Wessel for fruitful discussions. We thank H Moritz, F Gerbier, I Bloch and I Spielman for providing us the experimental data. We thank the Aspen Center for Physics and the Institute Henri Poincare-Centre Emile Borel for hospitality and support. We thank the Swiss National Science Foundation, MaNEP Switzerland, the CNRS, the network 'Triangle de la Physique', the DARPA OLE program and FWO Vlaanderen for financial support. Part of the simulations ran on the Hreidar cluster at ETH Zurich.

References

[1] Greiner M, Mandel O, Hänsch T W and Bloch I 2002 *Nature* **419** 51
[2] Bloch I, Dalibard J and Zwerger W 2007 *Preprint* 0704.3011
[3] Hofstetter W, Cirac J I, Zoller P, Demler E and Lukin M D 2002 *Phys. Rev. Lett.* **89** 220407
[4] Trebst S, Schollwöck U, Troyer M and Zoller P 2006 *Phys. Rev. Lett.* **96** 250402
[5] Bednorz J G and Mueller K A 1986 *Z. Phys.* B **64** 189
[6] Mandel O, Greiner M, Widera A, Rom T, Hänsch T W and Bloch I 2003 *Nature* **425** 937
[7] Reischl A, Schmidt K P and Uhrig G S 2005 *Phys. Rev.* A **72** 063609
[8] Ho T-L and Zhou Q 2007 *Phys. Rev. Lett.* **99** 120404
[9] Diener R B, Zhou Q, Zhai H and Ho T-L 2007 *Phys. Rev. Lett.* **98** 180404
[10] Gerbier F, Widera A, Fölling S, Mandel O, Gericke T and Bloch I 2005 *Phys. Rev. Lett.* **95** 050404
[11] Blakie P B and Porto J V 2004 *Phys. Rev.* A **69** 013603
[12] Rey A M, Pupillo G and Porto J V 2006 *Phys. Rev.* A **73** 023608
[13] Jaksch D, Bruder C, Cirac J I, Gardiner C W and Zoller P 1998 *Phys. Rev. Lett.* **81** 3108
[14] Greiner M 2003 *PhD Thesis* Ludwig-Maximilian University, Munich
[15] Fisher M P, Weichman P B, Grinstein G and Fisher D S 1989 *Phys. Rev.* B **40** 546
[16] Pollet L 2005 *PhD Thesis* Universiteit Gent Belgium, Online at http://www.nustruc.ugent.be/phdtheses.html
[17] Kühner, White S R and Monien H 2000 *Phys. Rev.* B **61** 12474
[18] Capogrosso-Sansone B, Söyler S G, Prokof'ev N V and Svistunov B V 2008 *Phys. Rev.* A **77** 020408
[19] Elstner N and Monien H 1999 *Phys. Rev.* B **59** 12184
[20] Schmidt K P, Reischl A and Uhrig G S 2006 *Eur. Phys. J.* D **38** 343
[21] Paredes B, Widera A, Murg V, Mandel O, Fölling S, Cirac I, Shlyapnikov G V, Hänsch T W and Bloch I 2004 *Nature* **429** 277
[22] Capogrosso-Sansone B, Prokof'ev N V and Svistunov B V 2007 *Phys. Rev.* B **75** 134302
[23] Prokof'ev N V, Svistunov B V and Tupitsyn I S 1998 *Zh. Eksp. Teor. Fiz.* **114** 570
Prokof'ev N V, Svistunov B V and Tupitsyn I S 1998 *Sov. Phys. –JETP* **87** 310
Prokof'ev N V, Svistunov B V and Tupitsyn I S 1998 *Phys. Lett.* A **238** 253
[24] Rombouts S M A, Van Houcke K and Pollet L 2006 *Phys. Rev. Lett.* **96** 180603
[25] Van Houcke K, Rombouts S M A and Pollet L 2006 *Phys. Rev.* E **73** 056703
[26] Wang F and Landau D P 2001 *Phys. Rev. Lett.* **86** 2050
[27] Zhou C and Bhatt R N 2005 *Phys. Rev.* E **72** 025701
[28] Troyer M, Wessel S and Alet F 2003 *Phys. Rev. Lett.* **90** 120201
[29] Kato Y, Zhou Q, Kawashima N and Trivedi N 2008 *Nature Phys.* to be published
[30] Werner F, Parcollet O, Georges A and Hassan S R 2005 *Phys. Rev. Lett.* **95** 056401
[31] Pollet L, Van Houcke K and Rombouts S M A 2007 *J. Comput. Phys.* **225** 2249
[32] Sandvik A W 1999 *Phys. Rev.* B **59** 14157
[33] Wessel S, Alet F, Troyer M and Batrouni G G 2004 *Phys. Rev.* A **70** 053615
[34] Bergkvist S, Henelius P and Rosengren A 2004 *Phys. Rev.* A **70** 053601

[35] Kinoshita T, Wenger T and Weiss D S 2004 *Science* **305** 1125
[36] Pollet L, Rombouts S M A and Denteneer P J H 2004 *Phys. Rev. Lett.* **93** 210401
[37] Wessel S, Alet F, Trebst S, Leumann D, Troyer M and Batrouni G G 2005 *J. Phys. Soc. Japan Suppl.* **74** 10
[38] Kollath C, Schollwöck U, von Delft J and Zwerger W 2004 *Phys. Rev.* A **69** 031601
[39] Fölling S, Widera A, Müller T, Gerbier F and Bloch I 2006 *Phys. Rev. Lett.* **97** 060403
[40] Kollath C, Köhl M and Giamarchi T 2007 *Phys. Rev.* A **76** 063602
[41] Gerbier F, Fölling S, Widera A and Bloch I 2007 *Preprint* cond-mat/0701420
[42] Stöferle T, Moritz H, Schori C, Köhl M and Esslinger T 2004 *Phys. Rev. Lett.* **92** 130403
[43] Günter K, Stöferle T, Moritz H, Köhl M and Esslinger T 2006 *Phys. Rev. Lett.* **96** 180402
[44] Gerbier F, Widera A, Fölling S, Mandel O, Gericke T and Bloch I 2005 *Phys. Rev.* A **72** 053606
[45] Spielman I B, Philips W D and Porto J V 2007 *Phys. Rev. Lett.* **98** 080404
[46] Gerbier F and Bloch I 2007 private communication
[47] Gerbier F 2007 *Phys. Rev. Lett.* **99** 120405
[48] Fölling S, Widera A, Müller T, Gerbier F and Bloch I 2006 *Phys. Rev. Lett.* **97** 060403
[49] Pollet L, Kollath C, Schollwöck U and Troyer M 2008 *Phys. Rev.* A **77** 023608
[50] Ospelkaus S, Ospelkaus C, Wille O, Succo M, Ernst P, Sengstock K and Bongs K 2006 *Phys. Rev. Lett.* **96** 180403
[51] Cramer M, Ospelkaus S, Ospelkaus C, Bongs K, Sengstock K and Eisert J 2007 *Preprint* 0707.3633
[52] Daré A-M, Raymond L, Albinet G and Tremblay A-M S 2007 *Phys. Rev.* B **76** 064402
[53] Koetsier A, Duine R A, Bloch I and Stoof H T C 2008 *Phys. Rev.* A **77** 023623